Ultrasonics Sonochemistry 76 (2021) 105662

Contents lists available at ScienceDirect

Ultrasonics Sonochemistry

journal homepage: www.elsevier.com/locate/ultson

Ultrasonic desulfurization of amphiphilic magnetic-Janus nanosheets in oil-water mixture system

Chunwei Shi [a,b,*], Xue Zhang [a], Xiaoyan Zhang [c], Ping Chen [a], Lingzi Xu [a]

[a] Liaoning Shihua University, Fushun 113001, China
[b] Administration Center of the Yellow River Delta Sustainable Development Institute of Shandong Province, Dongying 257001, China
[c] Liaoning Nuclear and Radiation Testing Center, Dalian 116107, China

ARTICLE INFO

Keywords:
Iron oxide
Desulphurization
Modification
Janus
Ultrasonic wave

ABSTRACT

Fe_3O_4 was obtained by reacting $FeCl_2$ and $FeCl_3$ with polyethylene glycol, and labeled onto a amphiphilic Janus nanosheet. It was confirmed by infrared spectroscopy, SEM, AFM and EDS that the Fe_3O_4 nanoparticles changed from hydrophilic to amphiphilic. The oxidative desulfurization performance of amphiphilic iron oxide was studied. Results showed that the Janus nanosheets labeled with Fe_3O_4 could significantly improve the removal rate of thiophene sulfide in simulated oil synergistically with ultrasonic waves, and the desulfurization rate could reach 100%. Further, the effect of ultrasound on the sensing ability of the oil–water interface was studied and the ultrasonic attenuation coefficient was calculated. In addition to the desulfurization mechanism of Fe_3O_4, it was found that although the ultrasonic attenuation coefficient of the amphiphilic nanosheets was high, the number of hydroxyl radicals determined the desulfurization efficiency. The amphiphilic Fe ions were more favorable for the formation of hydroxyl radicals than the single hydrophilic ones.

1. Introduction

China's major oil fields employ tertiary oil recovery processes, which include injection technology, technology for heavy oil, and thermal recovery. There is a need to add a variety of emulsifiers to maintain high oil–water emulsion stability of the oilfield wastewater [1]. Moreover the standards for sulfur content in fuel oil, produced from crude oil, are becoming more and more stringent [2]. Therefore, it is necessary to desulfurize the oil phase while separating the oil from water. Amongst the existing technologies for desulfurization, hydrodesulfurization has reached a higher industrial stage, but it fails to remove benzothiophene sulfide due to its steric effect [3–5]. Oxidative desulfurization, as a non-hydrodesulfurization technology, is especially suitable for deep desulfurization of oil–water systems due to its excellent selectivity, mild reaction conditions and strong adaptability to raw materials [6–8].

Solid Fe_3O_4 and H_2O_2 synergistically formed a Fenton-type reagent, which could oxidize and desulfurize the oil in a better manner, but the hydrophilic and oleophobic property of Fe_3O_4 limited its application in desulfurization in oil–water mixture. The use of an amphiphilic Janus material as the surfactant increased the contact of iron ions with the oil layer and hydrogen peroxide (water layer) , and improved the oxidative desulfurization efficiency of the Fenton-type reagent for oil–water mixture [9–13].

The stability of plate-like particles stabilized emulsion is higher than that of other structural particles [14]. Compared with spherical Janus particles, the rotation of Janus films with anisotropic structure at the emulsion interface is restricted, so the plate-like particles are more stable than the spherical particles in the shape of the emulsion.

Ultrasound-assisted desulfurization [15] of oil can obviously improve the desulfurization rate [16–18].Therefore, based on the Janus nanomaterials, this study marked the Janus nanosheets with Fe_3O_4, which gave oxidative properties to the Janus nanomaterials. This material realized the removal of sulfur from the oil–water system by means of ultrasonic waves, providing a theoretical basis for the efficient separation and treatment of oilfield wastewater.

2. Materials and methods

2.1. Reagents and instruments

Imidazoline-based Janus nanosheets were procured from the Institute of Chemistry, Chinese Academy of Sciences. Analytically pure dibenzothiophene was obtained from Sinopharm Chemical Reagent Co., Ltd. Analytically pure n-octane, methyl violet, hydrogen peroxide (30%

* Corresponding author.
E-mail address: chunweishilnpu@126.com (C. Shi).

https://doi.org/10.1016/j.ultsonch.2021.105662
Received 11 March 2021; Received in revised form 14 June 2021; Accepted 4 July 2021
Available online 7 July 2021

H_2O_2), and N, N-dimethylformamide were purchased from Shenyang Dongxing Reagent Factory.

Infrared spectra was recorded on a Bruker Equinox 55FT-IR infrared spectrometer (Bruker Beijing Technology Co., Ltd.). SEM images were obtained using a JSM6335 scanning electron microscope, JEOL. Thickness of nanosheets was determined by Asylum Research(AFM) MFP-3D-BIO(Oxford Instrument Technology (Shanghai) Co., Ltd.). The instrument to produce ultrasonic radiations was homemade [9]. The absorbances were recorded on a Tp-xos-type visible spectrophotometer (Tianjin Tuopu Instrument Co., Ltd.). Y-800 high shear homogenizer was used to mix the emulsion (Shanghai Shihe Instrument Co., Ltd.).

2.2. Experimental methods

2.2.1. Synthesis of Janus nanosheets [5]

The specific synthesis process is as follows [9]:The 15 mL styrene maleic anhydride copolymer aqueous solution (12 wt%) was mixed evenly in 80 mL deionized water, and the pH of the solution was adjusted to 2.5 by adding acetic acid. The aqueous solution was placed in a 75 °C water bath at constant temperature as the water phase (solution I). Take 25 g of paraffin and melt at 75 °C. Ethyl orthosilicate, aminopropyl trimethoxysilane and phenyl triethoxysilane with mass ratio of 5.6:1:4.5 were added into paraffin wax and mixed evenly (solution II). The solution I and II were mixed and shear emulsified at high speed with high shear homogenizer, the emulsification speed was 10000 rpm, the emulsification time was 6 min, the O/W emulsion was formed, and the emulsion reacted for 12 h at 75 °C. Hollow spheres were obtained after filtration, washing and drying. Janus nanosheets were prepared by grinding with colloid for 20 min.

2.2.2. Synthesis of Fe_3O_4 nanoparticles [7]

Prepare 100 mL 5 mol/L sodium hydroxide solution, deoxidize with nitrogen for 1 h, add 11 mL 0.5 mol/L $FeCl_2$ solution and 10 mL 1 mol/L $FeCl_3$ solution, stir for 1 h at room temperature, and the reaction is in the N_2 atmosphere. Then heat up to 900 °C, continue stirring for 1 h, add 100 mL 0.3 mol/L sodium citrate solution, continue stirring for 30 min, and finally precipitate with acetone. Fe_3O_4 nanoparticles were separated by magnet, washed with distilled water for many times and dried in vacuum.

2.2.3. Labeling of Janus nanosheets

The appropriate amount of Janus nanoparticles was dispersed in ethanol, 10 mg Fe_3O_4 nanoparticles were added, stirred for 30 min, and the Fe_3O_4 nanoparticles which were not adsorbed on Janus were removed. The results were observed by SEM.

2.2.4Preparation of simulated oil

Dibenzothiophene (0.8193 g) was weighed and dissolved in n-octane. It was diluted with n-octane to 50 mL, in a volumetric flask. It had a sulfur content of 7×10^{-4} mol/L.

2.3. Sample performance and characterization methods

Small amounts of each of the two samples (Fe_3O_4 and F-J) were mixed thoroughly with potassium bromide powder, which were then tableted and analyzed by infrared spectrometry. The morphology of Janus nanosheets was studied by scanning electron microscopy, which was performed on a copper mesh carbon film after ultrasonically dispersing in ethanol for 20 min.

2.4. Desulfurization performance evaluation

In a conical flask equipped with a condenser, hydrogen peroxide (30%, 4 mL), deionized water (4 mL), acetic acid (1 mL), H_2O_2(10 mL), F-J nanosheets (0.10 g), and simulated oil (8 mL) were added successively. The oil content of the mixture was about 50%. The mixture was placed in ultrasonic machine and reacted at 20 °C for 30 min. In the above conditions, F-J nanosheets (0.10 g) can be replaced by Fe_3O_4(0.10 g),(Formic acid(2 mL) + Sulfuric acid(2 mL)) [19].

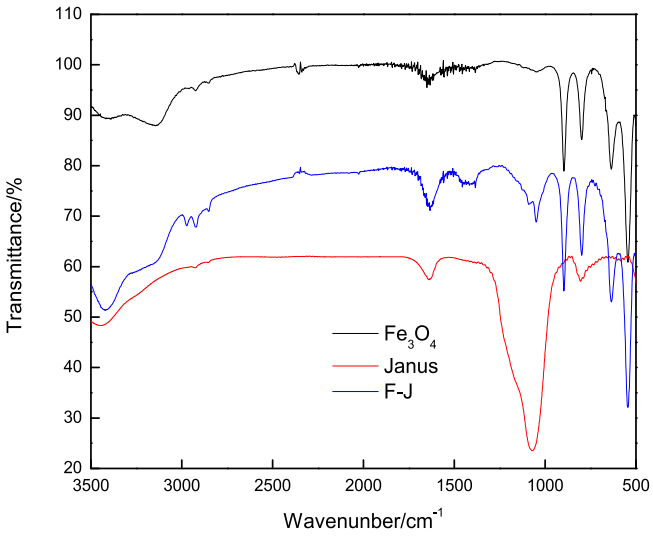

Fig. 1. IR spectra of three samples.

The experimental conditions without ultrasonic were as follows: In a conical flask equipped with a condenser, hydrogen peroxide (30%, 4 mL), deionized water (4 mL), acetic acid (1 mL), H_2O_2(10 mL), F-J nanosheets (0.10 g) (or Fe_3O_4(0.10 g)), and simulated oil (8 mL) were added successively. The oil content of the mixture was about 50%. The mixture was placed at 20 °C for 30 min with the homogenizer.

N, N-dimethylformamide (10 mL) was added and then extracted for 15 min. After standing for 10 min, the sulfur content was determined.

2.5. Determination of hydroxyl radicals

Then methyl violet solution (2 mmo1·L^{-1}, 0.5 mL) was added. The pH of the mixture was adjusted to 3.5. The blank sample was a mixture of hydrogen peroxide and n-octane

After reacting at room temperature for 10 min, the absorbance values of X and Y were measured spectrophoto metrically at 580 nm, with water as the reference. The absorbance was recorded asAtand the absorbance values of Z were recorded as A_0. The absorbance $\triangle A$ can be determined using the Eq. (1):

$$\triangle A = A_0\text{-}A_t \quad (1)$$

According to Lambert Beer's law (Eq. (2)):

$$\triangle A = \varepsilon \times b \times \triangle C \quad (2)$$

where, ε is the molar extinction coefficient or molar absorptivity; b is the length of the solution the light passes through (cm); and C is the concentration of the solution. The number of •OH generated is represented by $\triangle C$, which is proportional to $\triangle A$. Hence, the larger the value of ΔA, more is the concentration/ number of •OH [9].

3. Results and discussion

3.1. Characterization of Janus and F-J nanosheets

3.1.1. Infrared analysis

Fig. 1 shows the infrared spectra of Fe_3O_4, Janus nanosheets, and F-J samples. Comparison of the spectra shows that the modified Fe3O4 had the characteristic peaks of both, Fe_3O_4 and Janus nanosheets, which indicated that iron oxide was successfully labeled on the Janus nanosheets.

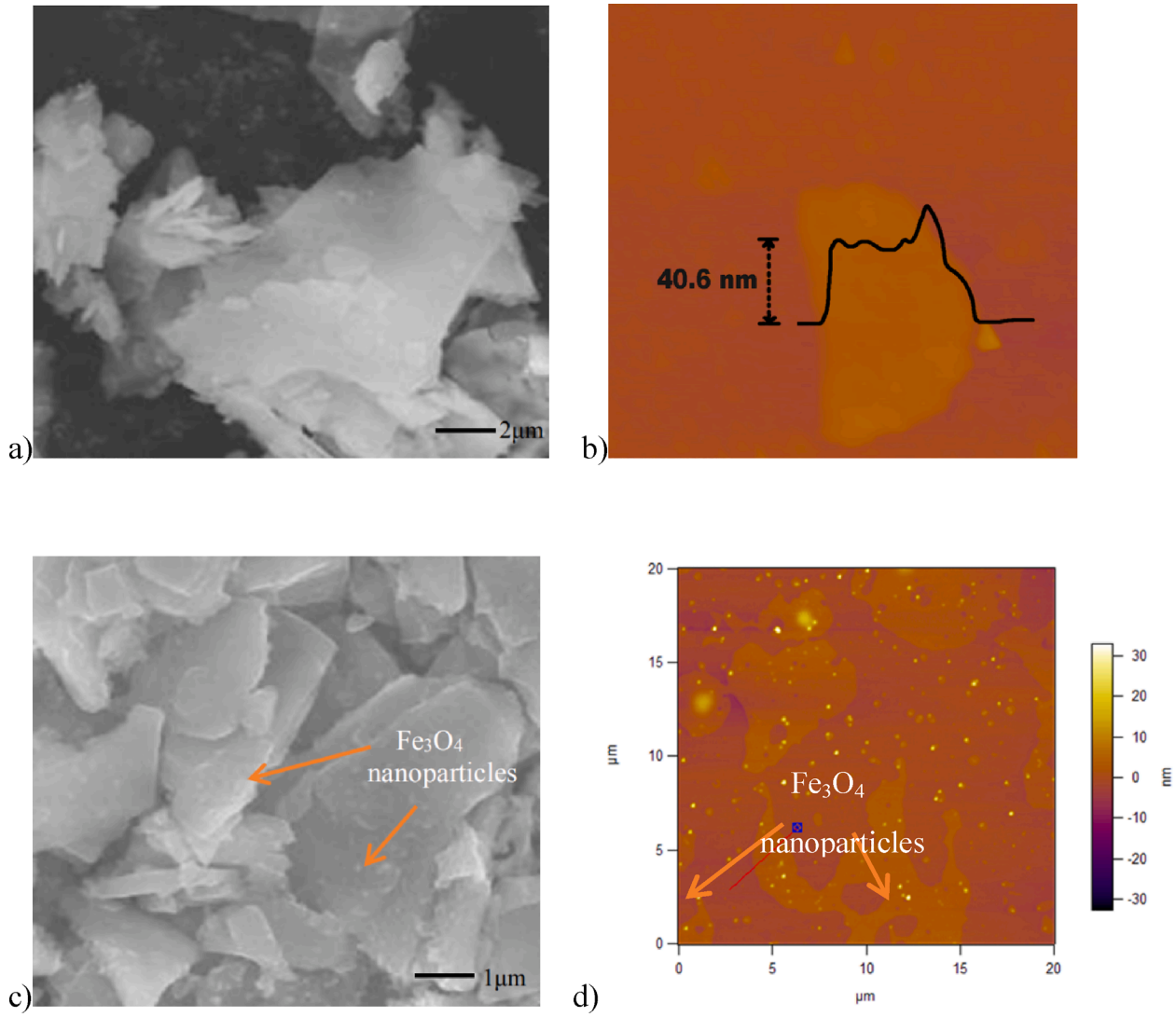

Fig. 2. SEM photos of nanosheets: a) and b)Janus;c) and d) F-J.

Table 1
EDX element analysis of Janus hollow sphere after being labeled with Fe_3O_4 nanoparticles.

Element	Si	O	N	C	Fe
Mass fraction/%	52.47	36.56	3.78	3.72	3.47

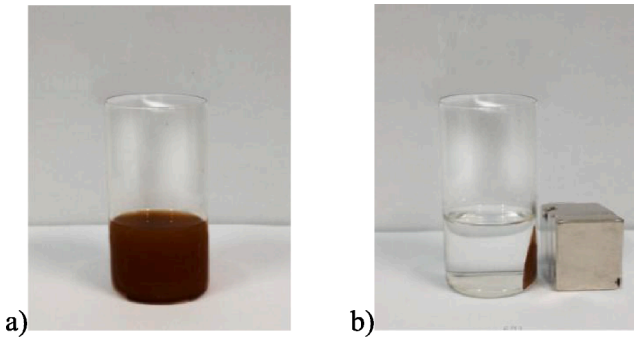

Fig. 3. Emulsification and demulsification of F-J nanosheets using simulated oil and water as oil/water phases:a)emulsification; b)demulsification.

3.1.2. *Surface topography analysis*

The Janus nanosheets were labeled with Fe_3O_4 nanoparticles (Fig. 2).Unloaded Janus nanosheets have a smooth surface and a thickness of about 40 nm. Fe_3O_4 nanoparticles were adsorbed on the side of Janus nanosheet with —NH_2 group, resulting in rough surface. Fe_3O_4 had prominence (Fig. 2(c)) and bright spot (Fig. 2(d)), and EDX analysis (Table 1) showed that there were Fe elements on Janus sheet with a mass fraction of 3.47%. It was proved that the prepared Janus sheet material was loaded with Fe_3O_4 nanoparticles.

3.1.3. *Emulsifying and demulsifying properties*

Fig. 3 shows that the F-J nanoparticles with amphiphilic properties can be mixed into emulsions with simulated oil and water evenly. After the magnetic field is applied, Fe_3O_4 is attracted by magnetic force, so that the emulsion is demulsifying and is easy to recover and separate.

3.2. *Ultrasonic attenuation coefficient*

Ultrasound is sensitive to oil–water interface [8,1,20]. Fe_3O_4 is hydrophilic, it forms oil–water stratified flow in the oil and water phases. While F-J is amphiphilic, so it forms oil in water core flow in the oil and water phases. Two different fluid systems lead to different ultrasonic attenuation coefficient. Therefore, it is necessary to examine the ultrasonic attenuation coefficients of the two systems.

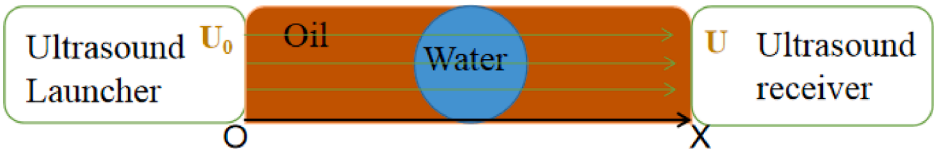

Fig. 4. Testing mechanism of ultrasonic attenuation.

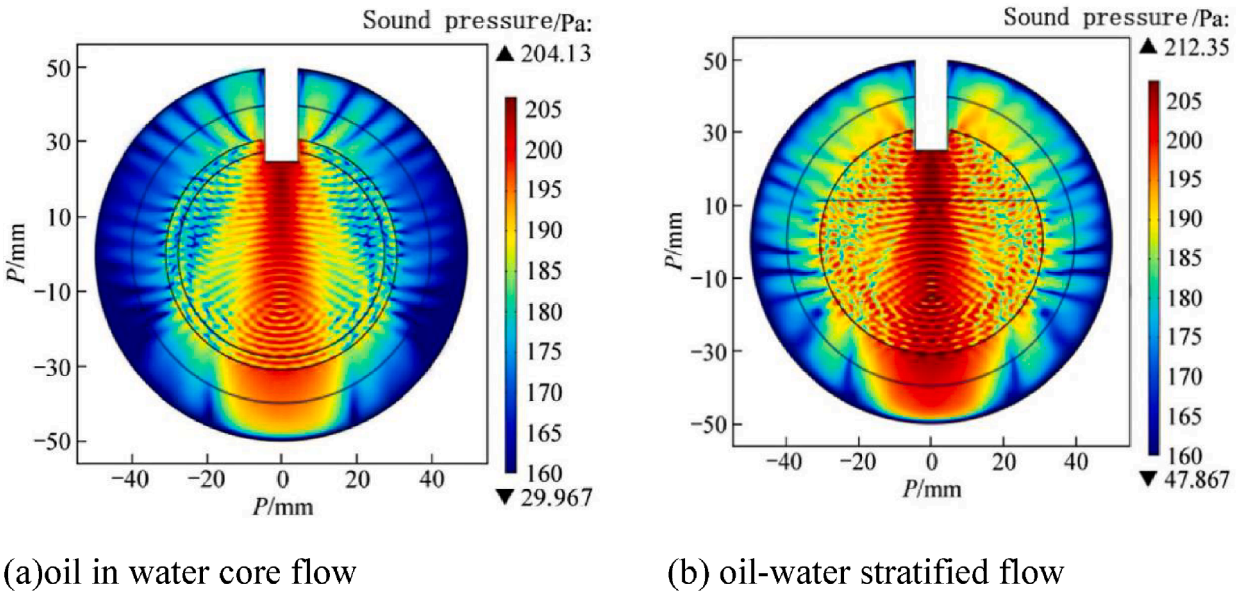

Fig. 5. Distributions of sound pressure in water-in-oil core flow.

The principle of ultrasonic measurement of oil–water biphasic flow was based on hydrodynamic and thermodynamic effects, which are shown in Fig. 4. The ultrasonic waves were emitted from the ultrasonic transmitting end with a certain frequency and intensity, which passed through the flowing oil–water phases. After phase absorption and other attenuation mechanisms, the ultrasonic waves reached the receiving end of the ultrasonic signal [3,16,20].

The ultrasonic attenuation coefficient can be determined using the Eq. (3):

$$\ln(U/U_0) = \ln(1 + R) - \alpha x \tag{3}$$

In Eq. (3), U_0 and U are the acoustic intensity (sound pressure) of the transmitting and receiving end of the ultrasonic wave respectively; R is the emission coefficient; α is the attenuation coefficient of the ultrasonic wave; x is the volume ratio of oil to water.

The transmitting end adopted the structural–acoustic coupling. The sensor had a diameter of 7 mm and the ultrasonic frequency transmitted was 500 kHz. The pressure of sound was 500 kPa. The receiving end received the attenuated signal through a two-dimensional intercept line.

The main simulation parameters were set as follows: temperature of 293.15 K, water density of 1000 kg•m^{-3}, water sound speed of 1500 m•s^{-1}, n-octane density of 703 kg•m^{-3}, and n-octane sound speed of 1300 m•s^{-1}. The simulation obtained the ultrasonic sound pressure distribution in the measured field (Fig. 5).

The ultrasonic attenuation coefficients of the two systems were measured. The value in Fig. 5 (a) was 12.08 dB•m^{-1}, which was larger than that in Fig. 5 (b) (7.95 dB•m^{-1}). This was due to the fact that in Fig. 5 (a) the oil–water interface and the transmitting end of the ultrasonic wave propagation direction was at a certain angle, there would be scattering effect, the attenuation loss of ultrasonic wave in addition to the propagation loss in the medium, the energy loss caused by scattering was relatively high. In Fig. 5 (b), because the propagation direction of ultrasonic wave was perpendicular to the oil–water interface, the scattering effect was relatively weak. The attenuation loss of ultrasonic wave was mainly the propagation loss in the medium, and the energy loss was relatively low. Therefore, to a large extent, the ultrasonic attenuation coefficient was affected by the distribution of oil and water two-phase medium.

Table 2
Comparison of desulfurization effectiveness in different reaction systems.

Desulphurization system	Desulphurization rate /%
F-J / ultrasonic	100%
Fe_3O_4/ ultrasonic	88%
Formic acid + sulfuric acid/Ultrasonic	79%
F-J	60%
Fe_3O_4	45%

3.3. Desulfurization ability

3.3.1. Desulfurization rate

In order to study the performance of oxidative desulfurization of Fe_3O_4, a comparative experimental study was designed. The reaction conditions and desulfurization effects are shown in Table 2.

The desulfurization effect on the reaction system on addition of 0.10 g F-J (0.03 g Fe_3O_4) and sonication was most obvious, which could reach 100%. On the other hand, ultrasonic desulfurization rate with 0.03 g of Fe_3O_4, Formic acid + sulfuric acid/ultrasound, only F-J and only Fe_3O_4 were 88%, 79%,60%,45%, respectively.

Obviously, ultrasonic desulfurization using F-J was more effective, which also indicated that ultrasonication promoted desulfurization. In this process, Fe_3O_4 was always present at the interface between the two phases, due to the amphiphilic nature of Janus. Under the action of ultrasonic waves, Fe ions with high catalytic activity, constantly promoted

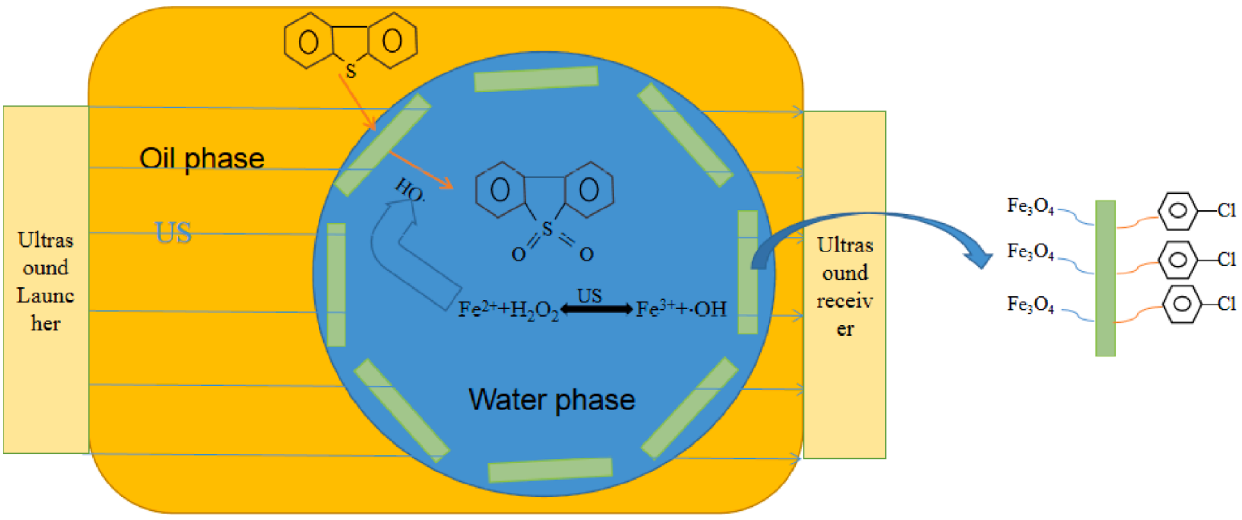

Fig. 6. The schematic diagram of oxidative desulfurization of F-J nanosheet at the interface. After ultrasonication for 30 min, dibenzothiophene was adsorbed and oxidized to polar disulfoxide at the oil–water interface, which was dissolved in the aqueous phase.

Table 3
Comparison of desulfurization effectiveness in different reaction systems.

System name	A	△A
The blank sample system	—0.004	0.004
Fe_3O_4 system	—0.058	0.058
F-J system	—0.069	0.069

the formation of hydroxyl radicals in hydrogen peroxide. Thiophene (non-polar) was oxidized to disulfoxide (polar), which then dissolved in water and was removed.

The schematic diagram for oxidative desulfurization of F-J nanosheets at the oil–water interface is shown in Fig. 6.

3.3.2. *Hydroxyl radicals*

Although the ultrasonic attenuation coefficient of the F-J system was large, its desulfurization effect was larger than that of the Fe_3O_4 system. This indicated that the ultrasonic attenuation phenomenon had little effect on desulfurization, under the premise that the ultrasonic intensity was satisfied. The oxidative desulfurization capacity of the system was determined by the number of hydroxyl radicals [1421–22].

According to the experimental method of 1.6, the principle was that methyl violet was purple in acidic solution with pH ≥ 3.0, and •OH could easily attack high electron density points. Therefore, •OH and —C = C— in methyl violet with high electron density could undergo an electrophilic addition reaction to cause the methyl violet to fade. The results of the changes in absorbances of the solutions after treatment with different systems are shown in Table 3.

It can be seen from Table 3 that the order of •OH content was consistent with the order of desulfurization rate, indicating that the

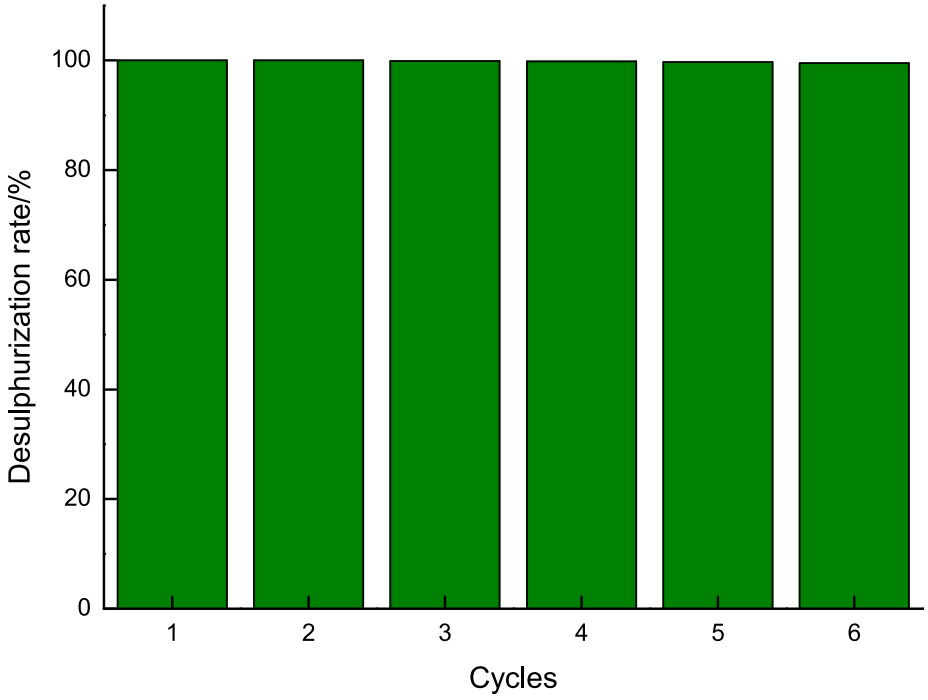

Fig. 7. Reuse performance of catalyst F-J.

number of •OH in the ultrasonic-Fe-oil–water system determined the desulfurization efficiency, and the amphiphilic Fe ion was more favorable for the generation of •OH free radicals.

3.3.3. Reuse performance

In industrial applications, recycling efficiency is an important index for evaluating the performance of a catalyst. For this reason, we take F-J nanosheets as an example to explore the reusability of F-J nanosheets in the process of emulsification oxidation desulfurization. The results are shown in Fig. 7. When the desulfurization experiment is finished, the demulsification of the desulfurization system is realized by applying an external magnetic field, and the upper oil phase is dumped. The catalyst F-J was added to the round-bottom flask, and the model oil was added to start the next cycle of ultrasonic-assisted desulfurization experiments. After five desulfurization experiments, the desulfurization rate remained 99.5%. The experimental results showed that the Janus nanosheets loaded with Fe_3O_4 could be achieved under the condition of self-stabilization during repeated experiments.

4. Conclusions

Fe_3O_4 was obtained by reacting $FeCl_3{\cdot}6H_2O$ with sodium acetate, glycol, ethylenediamine and labeled on the amphiphilic Janus nanosheet, which converted the hydrophilic nature of Fe_3O_4 to amphiphilic. The performance of oxidative desulfurization of modified iron oxide was studied. Experiments showed that the synergistic effects of F-J and ultrasound could significantly improve the removal rate of thiophene sulfide in simulated oil, and the desulfurization rate increased by 18%, which means that it could achieve 100% desulfurization.

The sensing ability of ultrasonic waves at the oil–water interface was studied and the attenuation coefficient was calculated. In addition to the desulfurization mechanism of Fe_3O_4, it was found that the •OH content determined the desulfurization efficiency, and the amphiphilic Fe ion was more favorable for the generation of •OH free radicals.

Declaration of Competing Interest

The authors declare that they have no known competing financial interests or personal relationships that could have appeared to influence the work reported in this paper.

Acknowledgments

This research was supported by Foundation of Liaoning Province Educational Committee [2017LQN002], Natural Science Foundation of Liaoning Province and the Talent Scientific Research LSHU Foundation [2016xjj-064].

References

[1] C. Tan, W. Dai, H. Wu, F. Dong, A conductance ring coupled cone meter for oil-water two-phase flow measurement, IEEE Sensors J. 14 (4) (2014) 1244–1252.
[2] S. Chunwei, C. Jianbin, W. Qingquan, L. Fuxin, Research progress of application of magnetic separation technology in oilfield sewage treatment, Appl. Chem. Ind. 25 (4) (2018) 65–69.
[3] C. Shi, W. Yang, J. Chen, X. Sun, W. Chen, H. An, Y. Duo, M. Pei, Application and mechanism of ultrasonic static mixer in heavy oil viscosity reduction, Ultrason. Sonochem. 37 (2017) 648–653.
[4] L. Fuxin, L. Bing, Y. Zhenzhong, Janus composites, Chinese PolymerBull. 8 (2016) 45–51.
[5] F. Liang, K.e. Shen, X. Qu, C. Zhang, Q. Wang, J. Li, J. Liu, Z. Yang, Inorganic Janus nanosheets, Angew. Chem. Int. Ed. 50 (10) (2011) 2379–2382.
[6] C. Guihua, B. Yu, G. Zhengguo, L. Wenliang, Q. Nannan, S. Toshifumi, K. Toyoji, D. Qian, Synthesis and characterization of Eu(III) complexes of modified D-glucosamine and poly(N-isopropylacrylamide), Mater. Sci. Eng. C-Mater. Biological Appl. 78 (2017) 603–608.
[7] H. Yang, F. Liang, X. Wang, Y. Chen, C. Zhang, Q. Wang, X. Qu, J. Li, D. Wu, Z. Yang, Responsive Janus composite nanosheets, Macromolecules 46 (7) (2013) 2754–2759.
[8] F. Jurlmale, V. Mundla, J. Kadambi, Development of A-scan ultrasound technique for measuring local particle concentration in slurry flows, Powder Technol. 215 (2012) 174–184.
[9] K. Kaurh, H. Halliwellb, Aromatic hydroxylation of phenyl nine as an assay for hydroxyl radicals, Anal Biochemist 220 (1994) 11–15.
[10] M. Nishants, G. Paragr, Intensified approach for desulfurization of simulated fuel containing thiophene based on ultrasonic flow cell and oxidizing agents, Ultrason. Sonochem. 51 (2019) 58–68.
[11] M. Qingbin, Y. Peng, F. Taiyang, J. Xinyang, Z. Qing, L. Dulin, W. Shenyang, L. Fuxin, Z. Zhenlin, S. Ximing, Phosphomolybdic acid-responsive Pickering emulsions stabilized by ionic liquid functionalized Janus nanosheets, J. Colloid Interface Sci. 507 (2017) 74–82.
[12] Q. Fan, G. Bai, Q. Liu, Y. Sun, W. Yuan, S. Wu, X.-M. Song, D.-Z. Zhao, The ultrasound thermal cracking for the tar-sand bitumen, Ultrason. Sonochem. 50 (2019) 354–362.
[13] R. Deng, F. Liang, P. Zhou, C. Zhang, X. Qu, Q. Wang, J. Li, J. Zhu, Z. Yang, Janus nanodisc of diblock copolymers, Adv. Mater. 26 (26) (2014) 4469–4472.
[14] H. Ruixia, L. Jitao, Z. Shuzhen, Molecular probe for the determination of hydroxyl radicals in heterogeneous systems: Coumarin, Chem. J. Chinese Universities 39 (12) (2018) 2658–2664.
[15] Y. Shaohua, P. Jiannan, J. Feng, L. Shiwei, P. Jinhui, Z. Libo, J. Shaohua, C. Srinivasakannan, Ultrasound-assisted leaching of rare earths from the weathered crust elution-deposited ore using magnesium sulfate without ammonia-nitrogen pollution, Ultrason. Sonochem. 41 (2018) 156–162.
[16] D. Tengyun, Q. Wenqian, W. Yadan, Pilot study of wave-number domain attenuation coefficient (W-Ac) for evaluation early liver fibrosis in vivo experiment, Acta Universitatis Medicinalis Anhui 53 (9) (2018) 1469–1472.
[17] W. Xinbi, Z. Ruixin, L. Xingpeng, L. Konghui, Preparation of rodlike iron oxide and its modification-ultrasonic desulfurization performance, J. Petrochemical Universities 31 (1) (2018) 30–36.
[18] Y. Yan, M. Li, D.i. Yang, Q. Wang, F. Liang, X. Qu, D. Qiu, Z. Yang, Construction of injectable double-network hydrogels for cell delivery, Biomacromolecules 18 (7) (2017) 2128–2138.
[19] S. Zhenbo, C. Zubin, H. Dongyun, Z. Rongxiang, Exploratory studyon ultrasonic oxidation desulfurization of catalytic cracking diesel oil, J. Liaoning Shihua University 36 (5) (2016) 10–14.
[20] Z. Yaoyao, W. Yueming, L. Bo, Study on measurement of fluid concentration in gas-solid two-phase flow by ultrasonic, Automation and Instruments 33 (4) (2019) 50–53.
[21] H. Yuge, W. Fei, L. Hongying, T. Chao, Y. Lei, Optimization on the extraction conditions of flavonoids from lactuca tatarica using response surface methodology, J. Liaoning Shihua University 39 (2) (2019) 21–25.
[22] C. Yujiu, Z. Xing, Removal of the typical products from lignocellulose acidolysis using Fenton reagent, Chem. Ind. Engin. Progress 37 (11) (2018) 4265–4270.